ARTICLE   OPEN

Contributions of external forcing and internal variability to the multidecadal warming rate of East Asia in the present and future climate

Dajeong Jeong [1], Changhyun Yoo [1 ✉] and Sang-Wook Yeh [2]

External forcing and internal variability contribute to multidecadal variation in the warming rate of East Asia. By rescaling the Coupled Model Intercomparison Project Phase 6 multi-model mean to the temperatures observed for the 1890–2020 period, we find that external forcing contributes about -0.2 to 0.1 K decade^{-1} to the warming rate until the 1980s, but this rate increases to 0.4 K decade^{-1} in recent decades. This multidecadal variation in the forced response is decomposed further into contributions by greenhouse gases, anthropogenic aerosols, and natural forcing. Once the external component is removed, the warming rate explained by the internal variability is ±0.15 K decade^{-1} in the twentieth century, reaching about -0.21 K decade^{-1} in recent decades. We find that 68% of the variance in the internally generated temperature anomaly is explained by the Indian Ocean Basin Mode (IOBM), the Atlantic Multidecadal Oscillation, and the Interdecadal Pacific Oscillation, with the IOBM playing a dominant role. In future Shared Socio-economic Pathway 2-4.5 scenario simulations, the impact of external forcing is projected to triple over the 2020–2100 period. Because the influence of internal variability remains relatively stable over this period, the contribution of external forcing becomes more pronounced in driving East Asian warming. These findings improve our understanding of both external and internal factors that shape trends and variation in the warming rate of East Asia and have implications for constraining future projections.

INTRODUCTION

The observed surface air temperatures over East Asia have shown a robust increase of more than 1 K over the past century[1,2]. As in other regions of the globe, increasing greenhouse gas (GHG) concentrations are the main driver of the multidecadal warming trend in East Asia, though the cooling effect of anthropogenic aerosol concentrations has offset some of this warming[2–4]. However, although GHG concentrations have been steadily increasing, the rate of change in the temperature over East Asia has varied from warming at about 0.4 K decade^{-1} to cooling at about -0.2 K decade^{-1} over the past century[5,6]. In addition, the recent slowdown in long-term warming has drawn attention to the influence of internal variability[7–10]. The importance of external and internal components differs depending on the region and period[11]. Thus, to better plan mitigation and adaptation strategies, we need to understand how sensitive East Asia's temperature is to external forcing and how much of its variance is driven by Earth's internal variability.

Accurately estimating the forced response is an important step in quantifying both external and internal contributions to a temperature time series. Statistical approaches can be used to estimate the response to external forcing[12]. One example is based on the linear relationship between the observed global surface air temperature and equivalent carbon dioxide concentrations[13]. This relationship is quite robust even at the continental scale, and the resulting forced response signal is not susceptible to model bias because the method uses only observations. However, its applicability at regional scales and when other types of forcing, such as aerosol forcing, are involved is not guaranteed. Another type of approach uses the multi-model mean (MMM) of several climate model simulations, assuming that freely evolving internal variability is uncorrelated between different realisations within a large ensemble[14–17]. Simulations in the Detection and Attribution Model Intercomparison Project[18] of the Coupled Model Inter-comparison Project Phase 6 (CMIP6)[19] allow us to estimate the role of each type of external forcing at each grid point. Nevertheless, a weakness of this approach is that the MMM is potentially biased compared to the degree to which the real world responds to external forcing. To account for potential differences between the amplitude of the true forced response and the MMM response, this study employs a semi-empirical approach by rescaling the MMM using the linear relationship between the MMM and observations[20–22]. We then apply the same method to each model simulation to identify the forced responses in each model, which vary greatly depending on how sensitive the model is to the forcing.

Once the forced signal is removed from the total temperature, the rest can be explained by the variability of freely evolving climate modes[5,20,23,24]. On a multidecadal time scale, three major climate modes play an important role in modulating the East Asian climate: the Atlantic Multidecadal Oscillation (AMO), Interdecadal Pacific Oscillation (IPO)[2,20,25–27], and Indian Ocean Basin Mode[28–30] (IOBM). For example, Miao et al.[20] showed that the internal component of East Asian temperatures is associated with the AMO and IPO, with correlation coefficients of -0.49 and 0.28, respectively. However, these correlations were not statistically significant at the 95% confidence level, and the IOBM, which we find to be dominant in the present study, was not included in their analysis.

[1]Department of Climate and Energy Systems Engineering, Ewha Womans University, Seoul, South Korea. [2]Department of Marine Science and Convergence Engineering, Hanyang University, ERICA, Ansan, South Korea. ✉email: cyoo@ewha.ac.kr
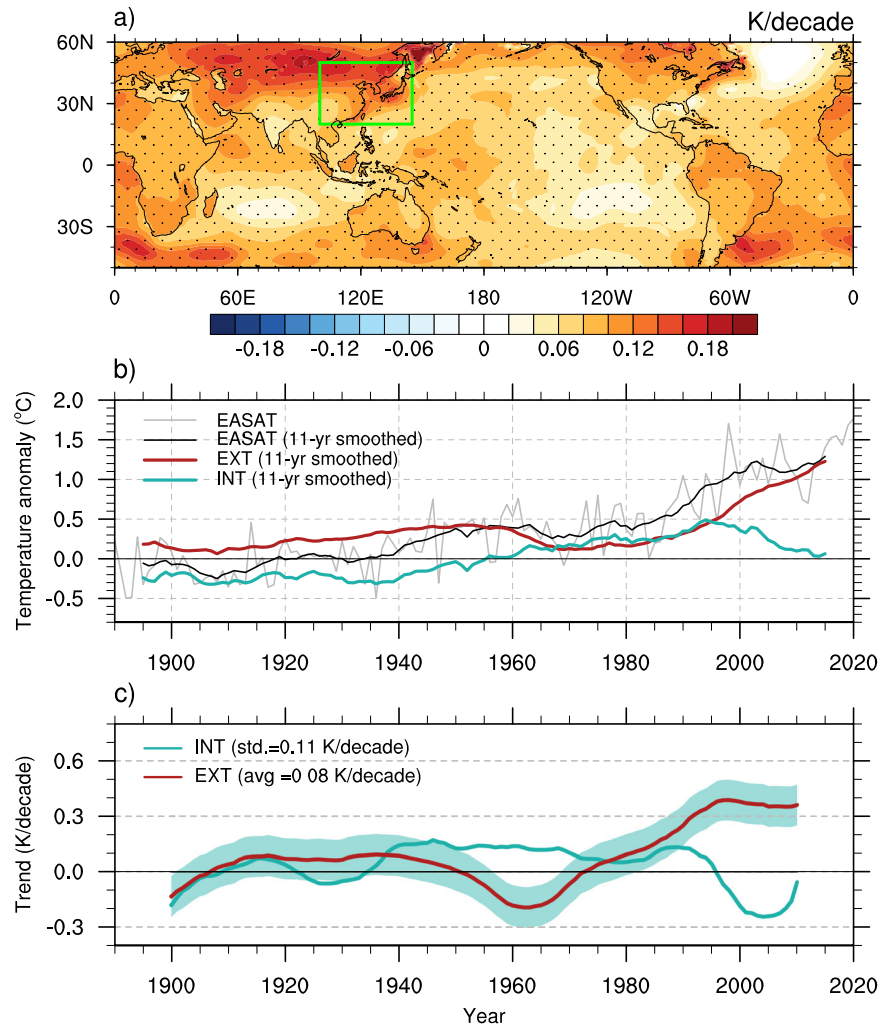
Fig. 1 Decomposition of the external and internal components. a Trend map for the temperature anomalies is shown in Kelvins per decade for the period from 1890 to 2020. The anomalies are obtained as the deviation from the climatology of the reference period 1900–1950. The green box indicates the East Asian domain (20°N–50°N, 100°E–145°E). The dotted regions indicate where the trends are statistically significant at the 95% level. **b** Temperature anomalies averaged over the East Asian domain (grey) are shown together with their 11-year running average (black). The externally forced component (EXT; red) and the internally generated component (INT; green) are derived from 11-year running averaged temperature anomalies. **c** 21-year running trend is used to estimate the temporal evolution of the externally forced (red line) and internally generated (green line) warming rates. The standard deviation of the internally generated component (0.11 K decade^{-1}) is added/subtracted (green shading) to produce the range for the East Asian warming rate.

This analysis is then applied to future scenario simulations to investigate whether and to what extent the relative amplitude of the forced response compared to the internal variability changes over the 2020–2100 period. This assessment can provide information on the extent to which future warming in East Asia can be mitigated by climate and air pollution policies. This analysis is also carried out for individual simulations to determine each model's sensitivity to forcing and uncertainty due to internal variability.

RESULTS

Contribution of external forcing and internal variability to the observed warming rate

Throughout the analysis period (1890–2020), warming has occurred globally, but has been more pronounced in East Asia (20 N°–50°N, 100E°–145°E) than in the rest of the world (Fig. 1a). While the global mean temperature has increased by about 0.09 K decade^{-1}, East Asia has experienced a higher warming rate of 0.11 K decade^{-1} (green boxed region in Fig. 1a; see also Fig. 2a in

Miao et al.[20]). The rate of warming has also varied between decades (e.g., Fig. 2a in Yao et al.[6]). For example, there has been a pause in the warming during some periods, such as the 1960s and the 2000s (grey line in Fig. 1b). This temporal behaviour remains apparent irrespective of whether the temperature anomalies are computed with 11-year running means (Supplementary Fig. 1c, d). These periods of paused warming can also be observed in the global mean temperature, as has been reported previously (Supplementary Fig. 1a, b and Fig. 1 in Yao et al.[6]). The cause of the temporal behaviour of the temperature in East Asia can be better understood by decomposing it into externally forced and internally generated components (red and green lines in Fig. 1b, respectively). As described in "Methods", the externally forced component is obtained by rescaling the MMM of all-forcing historical simulations (HIST) with the observations. The internally generated component of these observations is then obtained by subtracting the externally forced component from the total.

To quantify the warming rate driven by external forcing, we take the externally forced component (red line in Fig. 1b) and compute the Theil-Sen slope for a 21-year running window (red
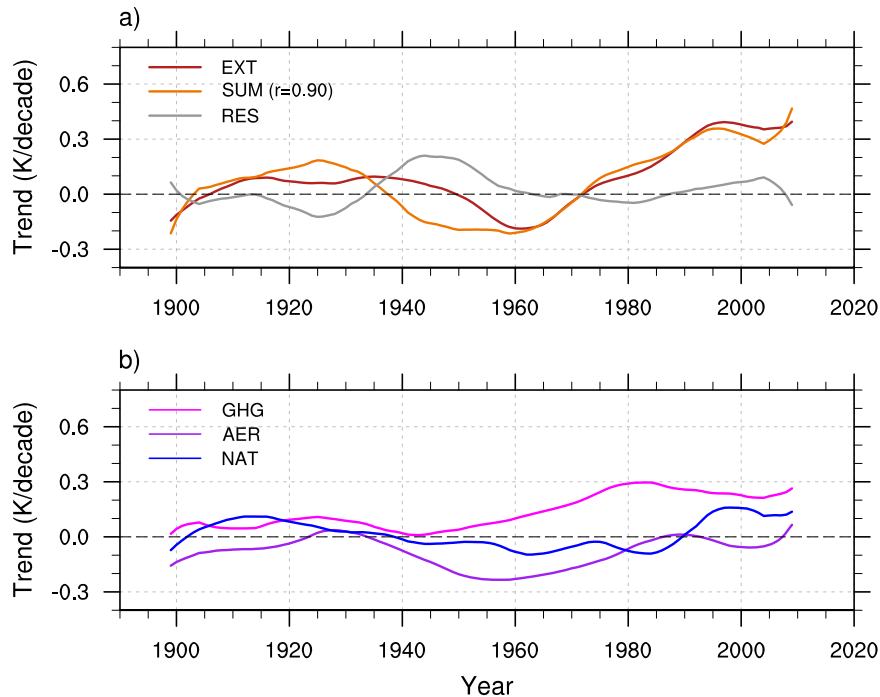
Fig. 2 Warming rates in East Asia driven by individual external forcings. a Externally forced component of the observed warming rate over East Asia (red; the same warming rate shown in Fig. 1c) is compared with the warming rate component derived by summing the individual forcings (orange). The Pearson correlation between the externally forced component and the sum is 0.90. The residual is defined by subtracting the derived sum from the total externally forced component. **b** Warming rates attributed to individual forcings, i.e., greenhouse gas (GHG; magenta), aerosol (AER; purple), and natural (NAT; blue) forcings.

line in Fig. 1c). This use of a running trend allows for continuous observations over the course of decades, instead of using warming rates measured for certain selected periods. We find that East Asia has consistently experienced warming due to external forcing over the entire analysis period except for the early twentieth century and the period from about the 1950s to the 1960s (red line in Fig. 1c). The externally forced warming rate varies from about -0.2 to $0.1\,K\,decade^{-1}$ until the 1980 but increases dramatically to about $0.4\,K\,decade^{-1}$ in recent decades.

We note that rescaling (red line) merely shifts the MMM temperature anomaly time series (blue line) to fit the observed time series (black line) without changing its shape (Supplementary Fig. 2). The original MMM minus the rescaled MMM is about $-0.2\,K$ throughout the study period (purple line). As a result, rescaling has a negligible effect on the warming rate; rather, it simply removes the centennial trend from the internally driven temperature anomaly (Supplementary Fig. 2b). This indicates that rescaling compensates for the underrepresented climate sensitivity of the MMM, i.e., an increase of about $1\,K$ over the entire period (blue line in Supplementary Fig. 2a), while the observations show a warming of about $1.2\,K$ (black line in Supplementary Fig. 2a). Without rescaling, there is long-term positive temperature responses due to internal variability (blue line in Supplementary Fig. 2b).

Internally generated variability can change the total warming rate in addition to the forced response. In the early twentieth century, the warming rate due to internal variability exhibits fluctuations of about $\pm 0.15\,K\,decade^{-1}$ (green line in Fig. 1c). A positive contribution persists in the mid to late twentieth century, but after the 1990s, it gradually decreases, reaching $-0.21\,K\,decade^{-1}$ in recent decades. We estimate the potential change associated with this freely evolving component by calculating its standard deviation over the entire period. By comparing this to the externally forced warming rate, we can compare the strength of the externally forced signal to the strength of this internal

noise[31,32]. The standard deviation has a value of $0.11\,K\,decade^{-1}$, which is comparable to the forced warming rate of East Asia. Adding a range of $\pm 0.11\,K\,decade^{-1}$ to the warming rate by the external forcing (shaded in Fig. 1c), we find that the internal variability substantially modulates the warming rate and determines whether it is positive or negative. However, as the warming rate by the external forcing has increased, the internal variability has not been sufficiently large since the 1980s to produce a negative warming rate in East Asia, which is consistent with recent studies[11].

Ignoring factors such as land use changes, the externally forced warming rate can be decomposed into the responses to historical GHG forcing, anthropogenic aerosol (AER) forcing, and natural (NAT) forcing (Fig. 2; see also "Methods"). The response to each type of forcing is calculated by taking the MMM of the single-forcing simulations without rescaling. This is because we do not have single-forcing observations and because rescaling has a negligible influence on the warming rate over East Asia (see Supplementary Fig. 2). To examine the accuracy of the decomposition, we also combine the three individually forced warming rates and compare this with the total warming rate. The sum of the three externally forced warming rates (orange line in Fig. 2a) reasonably reproduces the externally forced component (red line in Fig. 2a), with a correlation coefficient of about 0.90 ($p < 0.01$). The residual of the total warming rate minus the sum of the three warming rates (grey line in Fig. 2a) remains low except for the 1930–1960 period.

Consistent with our understanding, GHG forcing is the main driver of overall warming in East Asia, while AER forcing contributes to cooling (magenta and purple lines in Fig. 2b, respectively). The warming rate due to GHGs starts at about $0.1\,K\,decade^{-1}$ in the early twentieth century, increasing steadily to about $0.2\,K\,decade^{-1}$ in the late twentieth century. This increase is associated with a positive trend in GHG emissions because the temperature in East Asia has a linear relationship with equivalent
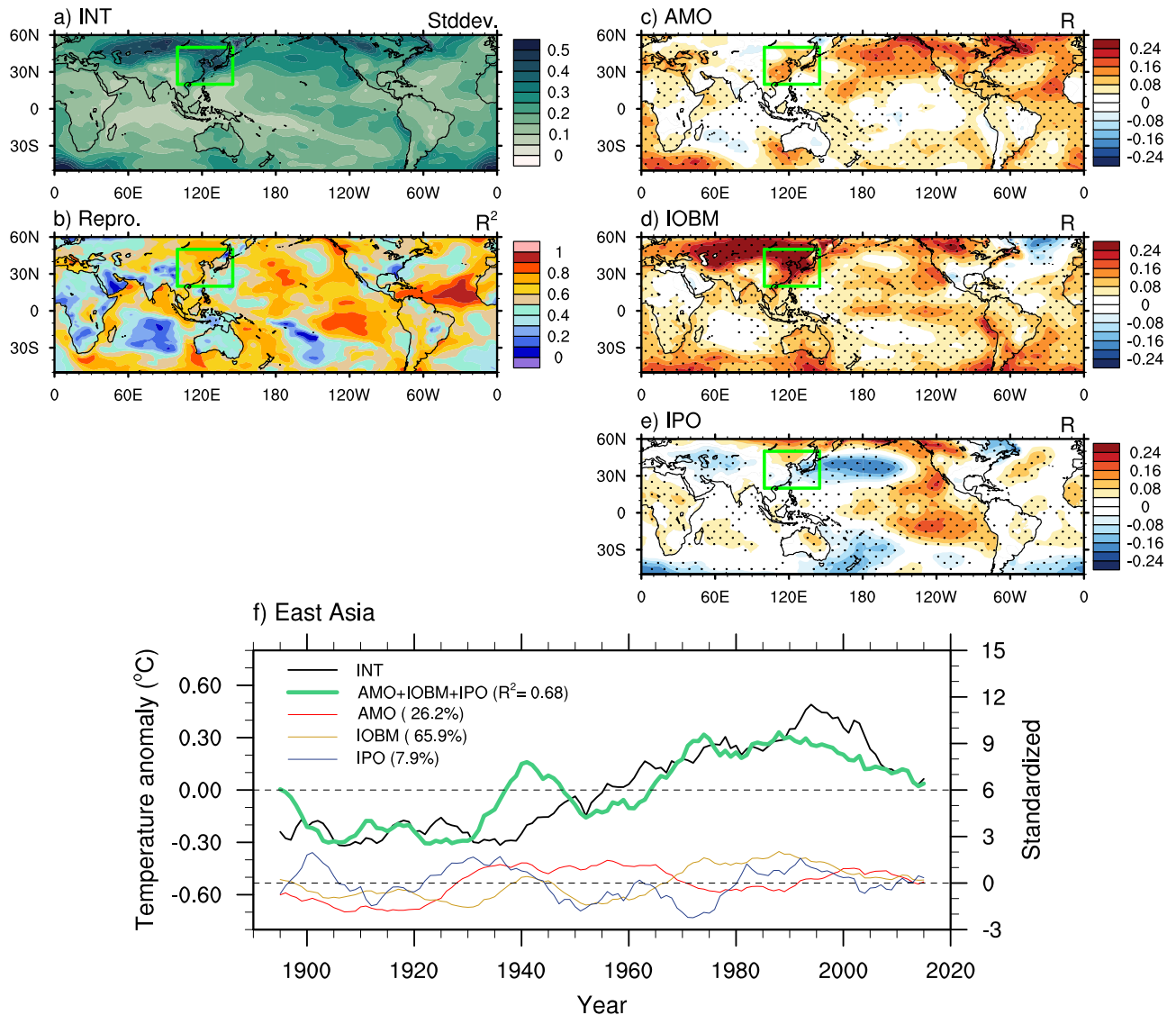
Fig. 3 Internal temperature variability and the role of climate modes. a Standard deviation is presented for the internal component (cf, green line in Fig. 1b) of the 11-year running average of the temperature anomalies at each grid point. This metric indicates the variation in temperature due to internal variability. The green box indicates the East Asian domain (20°N–50°N, 100°E–145°E). **b** Coefficient of determination is calculated between the reconstructed temperature anomalies from three climate modes—the Atlantic Multidecadal Oscillation (AMO), Indian Ocean Basin Mode (IOBM), and Interdecadal Pacific Oscillation (IPO)—and the observed internal temperature anomalies. Partial regression coefficients in the relationship between the internal temperature anomalies and the climate modes are shown for the (**c**) AMO, (**d**) IOBM, and (**e**) IPO. The dotted regions indicate where the regression coefficients are statistically significant at the 95% level. **f** 11-year running average of the internal variability of the temperature anomalies in East Asia (black; the green line in Fig. 1b), and the reconstruction derived from the three climate modes (green) are shown together with the standardised climate mode indices: AMO (red), IOBM (yellow), and IPO (blue). Their relative contributions, measured by their partial regression coefficients from a multiple linear regression model, are shown as percentages.

CO_2 (e.g., Fig. 2 in Wu et al.[13]). The warming rate due to AER forcing is about −0.2 K decade^{-1} in the 1960s and less than −0.1 K decade^{-1} in recent decades. The contribution of NAT forcing (blue line in Fig. 2b) has both positive and negative values, with some sporadic cooling periods during major volcanic eruptions (e.g., the Agung eruption in 1963 and the El Chichón eruption in 1982). When averaged over the entire period, the GHG-, AER-, and NAT-driven warming rates in East Asia are 0.13, −0.08, and 0.02 K decade^{-1}, respectively (Supplementary Fig. 3).

Having decomposed the total East Asian warming rate into its forced and internal components, and then further decomposing the forced components into individual forcing components, we now investigate the degree to which the internal variability of the East Asian warming rate is explained by the major multidecadal

climate modes, the AMO, IOBM, and IPO (see "Methods" for the definition of the climate modes). The internal variability, as measured using the standard deviation, is high over East Asia (Fig. 3a), surpassing that over the tropical eastern Pacific, the North Pacific, and the North Atlantic despite the presence of the IPO and the AMO. The partial regression coefficient between each climate mode and the near-surface temperature highlights the importance of the IOBM in explaining the internal variability in East Asia (Fig. 3c–e). The influence of the AMO is mainly observed in southern East Asia rather than over the whole of East Asia (Fig. 3c), while the IPO has a relatively weak influence on the internal variability of East Asian temperatures (Fig. 3e). The IOBM, on the other hand, tends to exhibit a warm Eurasia and cold Arctic-like pattern, meaning that it has a strong influence over East Asia

(Fig. 3d). The mechanism linking the IOBM to the East Asian climate can be understood through Rossby wave propagation[33]. This specific effect of the IOBM on the internal variability of temperatures in East Asia has not been reported in previous studies.

The internal component of East Asian temperature can be reproduced using the AMO, IOBM, and IPO indices as predictors in a multiple linear regression model (Fig. 3f). Here, the existing connection between the climate modes[34,35] is statistically removed when constructing the climate mode indices ("Methods"). The reconstructed temperature (green line) exhibits a strong correlation with observations (black line), with a correlation coefficient of 0.83 ($p < 0.01$). Thus, these three modes explain 68% of the internal variability in the temperature anomaly in East Asia. The relative contribution of each climate mode is measured as the ratio of each mode's partial regression coefficient to the sum of all partial regression coefficients in the multiple linear regression model built from the three standardised indices. This approach is made possible by the use of standardised and independent indices as predictors in multiple linear regression, allowing the partial regression coefficients to be interpreted as measures of the individual contributions of each predictor. Individually, the AMO, IOBM, and IPO account for 26.2%, 65.9%, and 7.9%, respectively, of the 68% variability. Thus, the IOBM is the largest contributor of the three indices to East Asian internal variability. When the same analysis is performed for each grid point (Fig. 3b), the spatial pattern of the variance explained by the three modes has features of the observed internal temperatures spread (Fig. 3a). The values of explained variance over the East Asian region range from 50% to 80%.

Future projections and model diversity
The present analysis estimates the contributions of individual types of forcing and variation due to multidecadal climate modes. Note that the separation of the forced response for the observation data was performed by rescaling the MMM to the observed temperature through linear regression analysis. The same analysis can also be conducted for the temperature time series in individual models by replacing the observed time series with historical simulations of the individual models. This allows the sensitivity of the individual models to forcing and the role of their internal variability to be estimated. In addition, this technique can be extended to future scenario and thus constrain the model bias in climate sensitivity.

The warming rates due to external forcing in the models vary substantially, averaging about 0.09 K decade^{-1} over the historical period (1890–2020), with a highest warming rate of about 0.12 K decade^{-1} and a lowest rate of about 0.06 K decade^{-1} (coloured markers in the HIST column of Fig. 4a). The observed forced warming rate, which is about 0.08 K decade^{-1} (black dot in Fig. 4a; see also the red line in Fig. 1c), falls well within the range of the modelled warming rates. Their range can be attributed to the sensitivity of the models to individual forcing types. For example, the decomposition of the individual models reveals significant variability in the warming rate attributed to GHGs (0.10–0.20 K decade^{-1}), AER (−0.13 to −0.05 K decade^{-1}), and NAT (all close to 0.01 K decade^{-1}) forcings (not shown).

We also estimate the variation in the warming rate that can be attributed to internal variability in East Asia using the standard deviation (Fig. 4b). The observed standard deviation over the historical period averages about 0.11 K decade^{-1} (black dot; see also green shading in Fig. 1c), with models showing a spread of about 0.06 K decade^{-1} in the standard deviation of the internal warming rate (0.09–0.15 K decade^{-1}). As mentioned above, the observed variation in the internal warming rate of East Asia can primarily be explained by the IOBM and the AMO, with a small contribution from the IPO. However, the relative contributions of the three climate modes differ considerably between the

individual models (not shown). This may be due to differences in the climate modes themselves and/or to the atmospheric/oceanic teleconnections in terms of how the impacts are conveyed to East Asia, but this is beyond the scope of the present study.

Extending the analysis to the Shared Socio-economic Pathway 2-4.5 (SSP245) future scenario, the models exhibit an increased warming rate (the SSP245 column in Fig. 4a), and we find a wider range for the forced warming rate between the individual models than across the historical period. The mean future warming rate is about 0.28 K decade^{-1}, while the models produce values of 0.20–0.40 K decade^{-1}, i.e., a range of about 0.20 K decade^{-1}. Compared to the warming rate of the historical period (0.09 K decade^{-1}), the projected values produced by the models are about 3.1 times higher. The forced warming rates for the individual models are also about 2.1–3.8 times higher than that for the historical period (Fig. 4a). This suggests that the sensitivity of the models to the different forcing types does not change substantially between the periods.

In the SSP245 simulations, despite a slight reduction of about 9%, the standard deviation for the internal variability remains similar at 0.10 K decade^{-1} (cross marks in Fig. 4b). The range for the standard deviation also remains similar between the two periods, increasing from about 0.06 K decade^{-1} in the historical simulations to 0.08 K decade^{-1} in SSP245 (the coloured markers in Fig. 4b) simulations. This suggests that there will be no substantial systematic changes in the contribution of the internal variability during future climate simulations. One possible reason for the marginal increase in the inter-model range may stem from a greater diversity of climate modes due to stronger external forcing in the future. This can be addressed by examining various scenarios in future research.

Figure 4c presents the ratio of the forced response to the internal variability. Because the internal variability remains stable while the forced response is projected to increase, the ratio increases from about 0.8 to 2.8, with a range of about 0.7 in the historical simulations increasing to about 3.9 in the SSP245 projections. This suggests that the sensitivity of individual models to external forcing will play a greater role in determining the rate of warming over East Asia in the future.

DISCUSSION
In this study, we investigate the relative contributions of external forcing and internal variability to multidecadal variation in the warming rate in East Asia between 1890 and 2020. The externally forced component is obtained by rescaling the MMM warming rate from 10 historical simulations of CMIP6 to the observed warming rate. The external component—which has values of about 0.1, −0.2, and 0.4 K decade^{-1} in the early, mid, and late twentieth century, respectively—explains the multidecadal variation in the warming rate. Because the internal component has a standard deviation of 0.11 K decade^{-1} during the 1890–2020 period, the relative contribution of external forcing increases substantially in the late twentieth century. When further decomposed into individual forcing components, the externally forced warming rate (0.08 K decade^{-1}) of the entire period is mainly driven by GHG warming (0.13 K decade^{-1}) and AER cooling (−0.08 K decade^{-1}), while NAT forcing plays a smaller role (0.02 K decade^{-1}). The internal variation is largely explained by the three major climate modes on a multidecadal time scale: the AMO, IOBM, and IPO. The variance explained by these three modes is about 68%, and the IOBM is the largest contributor to the internal East Asian warming rate. We postulate that although the magnitude of the warming rate and the contributions of the external forcing and internal modes may show some seasonality, the overall results are likely to remain the same.
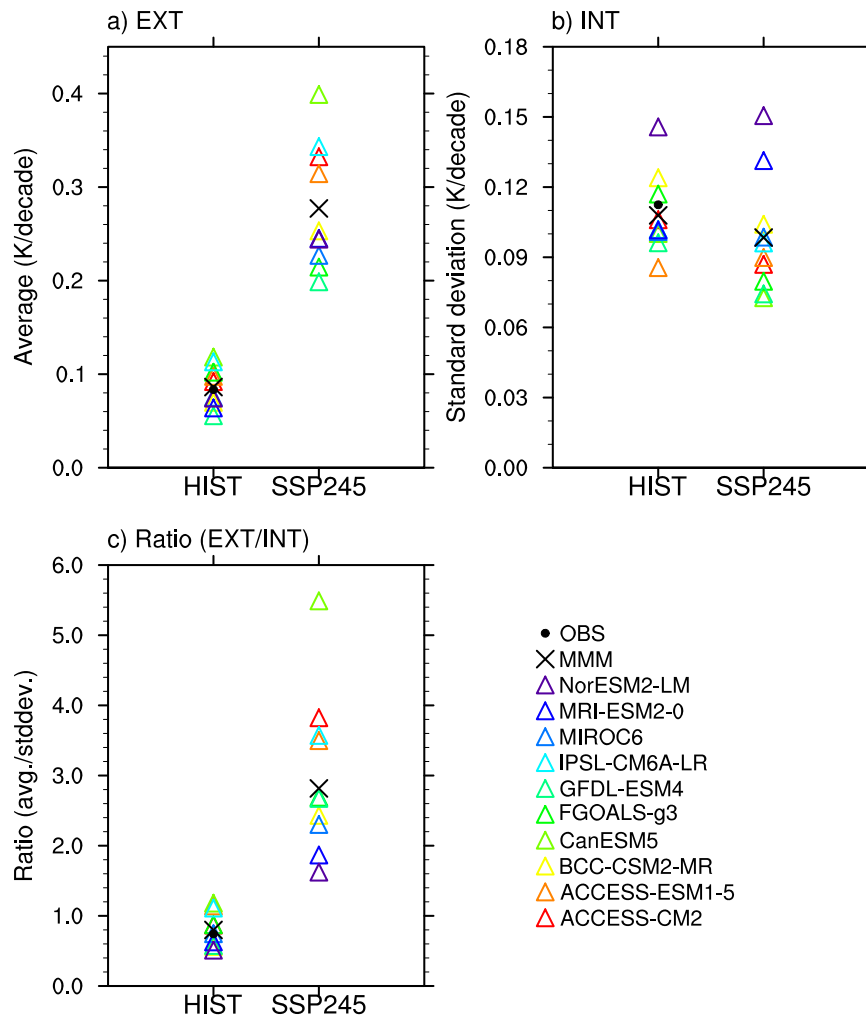
Fig. 4 Warming rates of individual models in the historical and future simulations. a Time mean warming rates due to external forcing are presented for historical (HIST; 1890–2020) and future (SSP245; 2020–2100) simulations. The observed, external warming rate (black dot) is obtained only for the HIST simulations. The model mean values are marked by black crosses. The warming rates of the individual models are represented by the coloured triangles. **b** Standard deviation of the internal variation components of the temperature are shown for the observations and the models. The ratio of (**a**) and (**b**) is shown in (**c**).

In future climate projections based on the SSP245 scenario, the impact of external forcing on the rate of warming in East Asia is expected to increase as the forcing becomes stronger, while the role of internal variability is expected to remain relatively similar. As a result, model sensitivity to external forcing will play an increasingly important role in determining the rate of warming over East Asia in the future. This suggests that, for more robust future projections, we need to accurately assess and improve the sensitivity of climate models so that their predictions match observations. This is particularly true for individual model projections. Compared to the average of model projection of about 0.28 K decade^{-1} warming for 2020–2100, the individual model projections exhibit a substantial range of 0.20–0.40 K decade^{-1}.

Our results highlight the importance of the IOBM and AMO and the more minor role of the IPO in the internal multidecadal variability of the warming rate in East Asia. However, in the models, the role of the AMO and IPO is relatively exaggerated compared to observations, while the opposite is true for the IOBM (not shown). If the influence of the AMO and IPO is primarily conveyed through atmospheric wave propagation, the discrepancy between the models and observations is likely due to the bias in the convective forcing associated with the modes and in

the background waveguide. This is an interesting subject but is beyond the scope of the present study. The relative importance of the climate modes may have implications for understanding decadal predictions using models, such as those used by the Decadal Climate Prediction Project.

It is important to note that our analysis of future projections focuses only on the SSP245 scenario. We can apply the same analysis to a range of future climate and air quality scenarios, such as those developed by the Aerosol Chemistry Model Intercomparison Project. This will provide valuable insights into future projected outcomes under different climate and air quality scenarios and will help inform the design of mitigation strategies on a continental or regional scale.

METHODS

Observational and model-simulated data

To investigate the role of external forcing and internal variability on the rate of warming in East Asia, we use the monthly near-surface air temperature data from the Berkeley Earth Surface Temperature (BEST) dataset[36]. We assess the credibility of BEST data in the East Asia region by comparing it with HadCRUT5[37], and our findings are consistent across both datasets (not shown). Due

to the lack of observations in the East Asia domain (20°N–50°N, 100°E–145°E) during the earlier period, this study analyses data from 1890 to 2020. To select a domain without any missing values (as in the polar regions), we calculate the global average of the variables by limiting the domain to a range of 60°S–60°N. As indices for oceanic climate modes, we use the sea surface temperatures (SSTs) from the Hadley Centre Global Sea Ice and Sea Surface Temperature[38] dataset. The SST data has the same horizontal resolution as the BEST data.

For the model simulations, we select 10 models, each with a single ensemble member from the CMIP6[19]. Based on our findings that the use of one ensemble member from each model produces results that are indistinguishable from those produced when employing up to 150 ensemble members, we choose to use only one ensemble member for each model for simplicity. The 10 models, listed in Supplementary Table 1, provide both HIST simulations and single-forcing simulations, i.e., GHG, AER, and NAT forcing. Because the historical simulations only cover the period up to 2014, we also use the SSP245 scenario simulations for 2015 to 2020 to match the observation period. Among the various SSP scenarios, SSP245 is chosen because it represents the intermediate GHG emissions scenario. For the future climate, we use the same SSP245 simulations from 2021 to 2100. To match the horizontal resolution, a 1° × 1° bilinear interpolation is conducted for all model datasets. In all models, we employ a land masked skin temperature as a representation of the SST.

Definition of climate modes

We use three major climate modes on a decadal to multidecadal timescale that are known to influence temperatures in East Asia: the AMO[39,40], IOBM[41], and IPO[42]. To account for interdecadal changes in internal variability, these climate modes are calculated using 11-year smoothed SST anomalies after removing the external forcing signal at each grid point. The AMO is calculated by averaging SST anomalies over the North Atlantic (0°–60°N, 0°–80°W)[43]. Similarly, the IOBM is calculated by averaging these over the entire Indian Ocean (45°S–20°N, 30°E–120°E)[33]. The IPO is calculated by subtracting the area mean of two regions, the northern Pacific (25°N–45°N, 140°E–145°W) and the southern Pacific (50°S–15°S, 150°E–160°W), from that of the eastern Pacific (10°S–10°N, 170°E–90°W)[44]. All indices are averaged using cosine-latitude-area weighting and standardised by their mean and variance.

To ensure the independence of each climate index, we compute the index and then remove the linear relationship between the computed index and SST anomalies. The next index is defined using the remaining SST anomalies, and this process is repeated for the third index. We choose to define the AMO first, followed by the IPO and then the IOBM. However, we find that our results are not sensitive to changes in the order in which the indices are calculated (not shown).

Quantification of externally forced and internally generated responses

To extract the temperature response to external forcing, we use the rescaled MMM[21,22]. To rescale the MMM, we linearly regress the temperature anomalies of the MMM against the actual temperature time series, where the actual temperature is obtained either from observations or the individual model simulations. Rescaling adjusts the amplitude differences between the actual forced response and the forced response obtained from the MMM. By applying this rescaled method, the average observed forced response increases by about 0.18 K compared to the MMM (Supplementary Fig. 2). The internal component is then obtained by removing the externally forced components from the total time series. Because our interest is in multidecadal trends and variability, we apply 11-year smoothing to the temperature anomalies. This 11-year window is subjectively chosen, but our

results are not sensitive to the window size when it is varied from 9 to 15 years (not shown).

The warming rate of the externally forced component is evaluated by the 21-year running trend of the Theil-Sen slope. This running trend is chosen to provide a continuous assessment of the warming rate that is not limited to a specific period. The 21-year window is chosen to cover a decadal timescale in accordance with previous studies[6,20]. We use the Theil-Sen slope to estimate the trend while minimising the effect of potential outliers. Our results remain robust to the use of a linear trend.

To measure the variation in the warming rate due to internal variability, we use the standard deviation of the internal component. The total variance is then explained by each climate mode (i.e., AMO, IOBM, and IPO) using the multiple linear regression model. Because the indices are all standardised, the relative size of the regression coefficients for each index is used to evaluate the relative role of each climate mode.

REFERENCES

1. Piao, S. L. et al. The carbon budget of terrestrial ecosystems in East Asia over the last two decades. *Biogeosciences* **9**, 3571–3586 (2012).
2. Wang, J. et al. Causes of East Asian temperature multidecadal variability since 850 CE. *Geophys. Res. Lett.* **45**, 13485–13494 (2018).
3. Allabakash, S. & Lim, S. Anthropogenic influence of temperature changes across East Asia using CMIP6 simulations. *Sci. Rep.* **12**, 11896 (2022).
4. Zha, J. et al. Contributions of external forcing and internal climate variability to changes in the summer surface air temperature over East Asia. *J. Clim.* **35**, 5013–5032 (2022).
5. Hua, W., Dai, A. & Qin, M. Contributions of internal variability and external forcing to the recent Pacific decadal variations. *Geophys. Res. Lett.* **45**, 7084–7092 (2018).
6. Yao, S.-L., Luo, J.-J., Huang, G. & Wang, P. Distinct global warming rates tied to multiple ocean surface temperature changes. *Nat. Clim. Change* **7**, 486–491 (2017).
7. Easterling, D. R. & Wehner, M. F. Is the climate warming or cooling? *Geophys. Res. Lett.* **36**, L08706 (2009).
8. Fyfe, J. C., Gillett, N. P. & Zwiers, F. W. Overestimated global warming over the past 20 years. *Nat. Clim. Change* **3**, 767–769 (2013).
9. Kosaka, Y. & Xie, S.-P. Recent global-warming hiatus tied to equatorial Pacific surface cooling. *Nature* **501**, 403–407 (2013).
10. Trenberth, K. E. & Fasullo, J. T. An apparent hiatus in global warming?. *Earths Future* **1**, 19–32 (2013).
11. Hua, W. et al. Reconciling human and natural drivers of the tripole pattern of multidecadal summer temperature variations over Eurasia. *Geophys. Res. Lett.* **48**, e2021GL093971 (2021).
12. Frankignoul, C., Gastineau, G. & Kwon, Y.-O. Estimation of the SST response to anthropogenic and external forcing and its impact on the Atlantic Multidecadal Oscillation and the Pacific Decadal Oscillation. *J. Clim.* **30**, 9871–9895 (2017).
13. Wu, T., Hu, A., Gao, F., Zhang, J. & Meehl, G. A. New insights into natural variability and anthropogenic forcing of global/regional climate evolution. *npj Clim. Atmos. Sci.* **2**, 18 (2019).
14. Dai, A. & Bloecker, C. E. Impacts of internal variability on temperature and precipitation trends in large ensemble simulations by two climate models. *Clim. Dyn.* **52**, 289–306 (2019).
15. Deser, C., Knutti, R., Solomon, S. & Phillips, A. S. Communication of the role of natural variability in future North American climate. *Nat. Clim. Change* **2**, 775–779 (2012).

16. Hawkins, E. & Sutton, R. The potential to narrow uncertainty in regional climate predictions. *Bull. Am. Meteorol. Soc.* **90**, 1095–1108 (2009).

17. Meehl, G. A., Arblaster, J. M., Fasullo, J. T., Hu, A. & Trenberth, K. E. Model-based evidence of deep-ocean heat uptake during surface-temperature hiatus periods. *Nat. Clim. Change* **1**, 360–364 (2011).

18. Gillett, N. P. et al. The Detection and Attribution Model Intercomparison Project (DAMIP v1.0) contribution to CMIP6. *Geosci. Model Dev.* **9**, 3685–3697 (2016).

19. Eyring, V. et al. Overview of the Coupled Model Intercomparison Project Phase 6 (CMIP6) experimental design and organization. *Geosci. Model Dev.* **9**, 1937–1958 (2016).

20. Miao, J. & Jiang, D. Multidecadal variations in East Asian winter temperature since 1880: internal variability versus external forcing. *Geophys. Res. Lett.* **49**, e2022GL099597 (2022).

21. Steinman, B. A., Mann, M. E. & Miller, S. K. Atlantic and Pacific multidecadal oscillations and Northern Hemisphere temperatures. *Science* **347**, 988–991 (2015).

22. Dai, A., Fyfe, J. C., Xie, S.-P. & Dai, X. Decadal modulation of global surface temperature by internal climate variability. *Nat. Clim. Change* **5**, 555–559 (2015).

23. Jiang, J., Zhou, T., Chen, X. & Zhang, L. Future changes in precipitation over Central Asia based on CMIP6 projections. *Environ. Res. Lett.* **15**, 054009 (2020).

24. Wang, J. et al. Internal and external forcing of multidecadal Atlantic climate variability over the past 1,200 years. *Nat. Geosci.* **10**, 512–517 (2017).

25. Hao, X. & He, S. Combined effect of ENSO-like and Atlantic multidecadal oscillation SSTAs on the interannual variability of the East Asian winter monsoon. *J. Clim.* **30**, 2697–2716 (2017).

26. Li, S. & Bates, G. T. Influence of the Atlantic multidecadal oscillation on the winter climate of East China. *Adv. Atmos. Sci.* **24**, 126–135 (2007).

27. Monerie, P.-A., Robson, J., Dong, B. & Hodson, D. Role of the Atlantic multidecadal variability in modulating East Asian climate. *Clim. Dyn.* **56**, 381–398 (2021).

28. Kim, S. & Kug, J.-S. Delayed impact of Indian Ocean warming on the East Asian surface temperature variation in Boreal summer. *J. Clim.* **34**, 3255–3270 (2021).

29. Liu, S. & Duan, A. Impacts of the leading modes of tropical Indian Ocean sea surface temperature anomaly on sub-seasonal evolution of the circulation and rainfall over East Asia boreal spring summer. *J. Meteorol. Res.* **31**, 171–186 (2017).

30. Sun, B., Li, H. & Zhou, B. Interdecadal variation of Indian Ocean basin mode and the impact on Asian summer climate. *Geophys. Res. Lett.* **46**, 12388–12397 (2019).

31. Hawkins, E. et al. Observed emergence of the climate change signal: from the familiar to the unknown. *Geophys. Res. Lett.* **47**, e2019GL086259 (2020).

32. Scaife, A. A. & Smith, D. A signal-to-noise paradox in climate science. *npj Clim. Atmos. Sci.* **1**, 28 (2018).

33. Zhang, Z., Sun, X. & Yang, X.-Q. Understanding the interdecadal variability of East Asian summer monsoon precipitation: joint influence of three oceanic signals. *J. Clim.* **31**, 5485–5506 (2018).

34. Cai, W. et al. Pantropical climate interactions. *Science* **363**, eaav4236 (2019).

35. Li, X., Xie, S.-P., Gille, S. T. & Yoo, C. Atlantic-induced pan-tropical climate change over the past three decades. *Nat. Clim. Change* **6**, 275–279 (2016).

36. Rohde, R. A. & Hausfather, Z. The Berkeley Earth land/ocean temperature record. *Earth Syst. Sci. Data* **12**, 3469–3479 (2020).

37. Morice, C. P. et al. An updated assessment of near-surface temperature change from 1850: the HadCRUT5 Data Set. *J. Geophys. Res. Atmos.* **126**, e2019JD032361 (2021).

38. Rayner, N. A. et al. Global analyses of sea surface temperature, sea ice, and night marine air temperature since the late nineteenth century. *J. Geophys. Res. Atmos.* **108**, 4407 (2003).

39. Kerr, R. A. A North Atlantic climate pacemaker for the centuries. *Science* **288**, 1984–1985 (2000).

40. Mann, M. E., Steinman, B. A. & Miller, S. K. On forced temperature changes, internal variability, and the AMO. *Geophys. Res. Lett.* **41**, 3211–3219 (2014).

41. Klein, S. A., Soden, B. J. & Lau, N.-C. Remote sea surface temperature variations during ENSO: evidence for a tropical atmospheric bridge. *J. Clim.* **12**, 917–932 (1999).

42. Power, S., Casey, T., Folland, C., Colman, A. & Mehta, V. Inter-decadal modulation of the impact of ENSO on Australia. *Clim. Dyn.* **15**, 319–324 (1999).

43. Trenberth, K. E. & Shea, D. J. Atlantic hurricanes and natural variability in 2005. *Geophys. Res. Lett.* **33**, L12704 (2006).

44. Henley, B. J. et al. A tripole index for the interdecadal Pacific oscillation. *Clim. Dyn.* **45**, 3077–3090 (2015).

AUTHOR CONTRIBUTIONS

D.J. and C.Y. designed the analyses, and D.J. performed the calculations. D.J. and C.Y. wrote the first draft and D.J., C.Y. and S.-W.Y. edited the manuscript.

COMPETING INTERESTS

The authors declare no competing interests.

ADDITIONAL INFORMATION

Supplementary information The online version contains supplementary material available at https://doi.org/10.1038/s41612-024-00573-w.

Correspondence and requests for materials should be addressed to Changhyun Yoo.

Reprints and permission information is available at http://www.nature.com/reprints

Publisher's note Springer Nature remains neutral with regard to jurisdictional claims in published maps and institutional affiliations.